A Graphite Orificed Hollow Cathode for an Argon Magnetoplasmadynamic Thruster

Jack Hollingsworth, '17

Submitted to the
Department of Mechanical and Aerospace Engineering
Princeton University
in partial fulfillment of the requirements of
Undergraduate Independent Work.

Final Report

May 3, 2017

Edgar Choueiri
Mikko Haataja
MAE 442
58 pages
File Copy

This thesis represents my own work in accordance with University regulations.

Abstract

An orificed hollow cathode with a lanthanum hexaboride insert is implemented for an argon-fed magnetoplasmadynamic thruster (MPDT) to investigate cathode life extension technology. The design of the cathode is developed and justified, and the design of an accompanying thruster for test purposes is detailed. Finite element models are built to ensure the thermal and static stability at steady-state of the operating thruster. Upon firing, it is found that the cathode ablates at a much higher rate with the lanthanum hexaboride insert than without it present. This may be due to a number of confounding factors, including water vapor retention, too-dense current densities, or mass transfer onto the insert. Further research is warranted into graphite orificed hollow cathodes, especially in regards to keeper technology, to prevent ion bombardment and improve cathode life.

Acknowledgements

While it may be my name on the cover of this thesis, none of these pages would have been possible without help from many people.

To Professor Choueiri: Thank you for welcoming me into your lab not once but twice, each time trusting my research skills and inspiring me to grow as a researcher and engineer.

To Will Coogan: Thank you for offering me the chance to join you in your research for my thesis. Thank you for your time, your patience, your guidance, your wit, your work ethic, and your comprehensive knowledge of MPDs, all given freely and without hesitation, as they have all taught me more than any class could have.

To the other members of the EP Lab: Thank you for welcoming me into your lab and taking an interest in me and what I was doing. Pierre-Yves, Chris, Matthew, and Sebastián, it was truly a pleasure to spend time with and learn from you all.

To my MAE friends: I can't thank you enough for keeping me sane during the many late nights and for making my four years here not just bearable but sometimes enjoyable.

To Josh, Guillermo, Evan, Agastya, Nate, Ginny, and Cai: I'm proud to call you all my friends. Cheers to die Spelmänner, and here's to many more family dinners.

Lastly, to Mom and Dad: your constant devotion and support does not go unnoticed or unappreciated. Thank you for everything you have done for me.

This thesis was made possible by a generous grant from the Morgan W. McKinzie Senior Thesis Fund and the Department of Mechanical and Aerospace Engineering.

Contents

List of Tables

List of Figures

Chapter 1

Introduction

Orificed hollow cathodes represent a promising way to increase thruster life for electric propulsion of spacecraft. This section introduces electric propulsion, makes the case for it, describes the benefits of hollow cathodes, and reviews prior investigations into hollow cathodes for magnetoplasmadynamic thrusters.

1.1 Why Electric Propulsion?

Electric propulsion, or EP, helps reduce the impact of large fuel payloads on deep-space travel. At present, long-distance space travel is hampered by the enormous amounts of propellant that conventional chemical rockets require to make the necessary velocity changes. The Tsiolkovsky rocket equation [6] illustrates this fundamental problem. As shown in Equation 1.1.1,

$$\Delta V = I_{\mathrm{sp}} g_0 \ln \frac{m_0}{m_{\mathrm{f}}} \tag{1.1.1}$$

where ΔV is the change in velocity due to the burn, I_{sp} is the specific impulse of the rocket, g_0 is the acceleration due to gravity on the Earth's surface, and $\frac{m_0}{m_f}$ is the ratio of the mass of the spacecraft plus propellant to the mass of the spacecraft. For a given I_{sp}, one can see that ΔV varies with the natural logarithm of the mass ratio of propellant ($\frac{m_0}{m_e}$). If we take, for example, a trip from low Earth orbit (LEO) to Mars orbit, we find that the minimum ΔV required to get there is 5.672 km/s. To leave LEO and enter the transfer orbit requires a ΔV of 3.573 km/s, while leaving the transfer orbit and entering orbit around Mars requires a ΔV of 2.099 km/s. Knowing that a typical I_{sp} for chemical rockets is about 450 s, we can compute the mass of

propellant required for the forementioned mission using each propulsion method using Equation 1.1.1 repeatedly. Rewriting in favor of the mass fraction, or percent of total rocket weight that must be fuel, we find that

$$M_{\mathrm{f}} = \frac{m_{\mathrm{f}}}{m_{\mathrm{f}} + m_{\mathrm{e}}} = \frac{1}{\exp\left(\frac{\Delta V_1}{I_{\mathrm{sp}} g_0}\right)\left(\exp\left(\frac{\Delta V_2}{I_{\mathrm{sp}} g_0}\right) - 1\right)} \tag{1.1.2}$$

where ΔV_1 is the ΔV of the Earth-escape maneuver and ΔV_2 is the ΔV of the transfer-Mars capture maneuver. Plugging in, we find that the mass fraction is equal to .498. Approximately half the rocket must be fuel in order to make it to Mars; this imbalance only gets worse with increasing values of ΔV and with increasing numbers of orbit changes, as the amount of mass compounds exponentially with each orbit change. Therefore, if complicated missions are to go to the outer reaches of the Solar System or beyond, a new propulsion method is necessary.

Electric propulsion (EP) is a useful alternative to chemical propulsion for spacecraft on long-distance journeys. The I_{sp} of EP thrusters is an order of magnitude greater than that of chemical rockets; therefore, a comparable mission using EP will require much less propellant for the same amount of ΔV. Using the previous example, and plugging in an I_{sp} of 4500 s, we find a mass fraction equal to .081. This is an eightfold reduction in the amount of propellant required to get our payload to Mars from LEO. Logically, it follows that for a given amount of propellant, EP will get the payload further than chemical propulsion. Therefore, if we want to go further from the Earth than chemical propulsion can take us, we need EP.

1.2 Magnetoplasmadynamic Thrusters

One promising type of electric thruster currently under development is the magnetoplasmadynamic (MPD) thruster. The MPD thruster accelerates ionized propellant electromagnetically to produce thrust. In doing so, the thrust-limiting factor ceases to be the chemical energy put out by the propellant and instead becomes the amount of electric power the spacecraft can deliver. The promise of MPDs lie in their high thrust density — an MPD thruster generates more thrust per unit mass than Hall or ion thrusters, which reduces time of transit for a given ΔV. [6] There are two types of MPDs, called self-field and applied-field MPDs. Self-field MPDs are preferable, as they have the highest of all thrust densities, but they require megawatts of power; as this is not yet feasible in a spacecraft, research is mainly conducted on applied-field

MPDs, which can achieve high efficiencies under 200 kW. [6]

The life-limiting component in all currently space-rated electric propulsion systems is the cathode. Cathodes in MPDs are the location of electron emission and of ion reception; this partially explains why the cathode is the shortest-lived of the MPD's components. The cathode is the electron emitter in an MPD thruster, and as a result it is also the ion receptor. Therefore, the cathode is constantly being bombarded by high-energy ions, which causes sputtering, or the loss of material due to collisions with highly energetic particles. [4]

Furthermore, the cathode has to carry the same amount of current as the anode, but through a much smaller cross-sectional area; therefore, the cathode will be hotter than the anode, and generally hotter than the rest of the thruster. This means that the cathode will evaporate before the anode. As no other components are consumed other than propellant, the combination of sputtering and evaporation leads to a cathode lifespan much shorter than any other part on the thruster.

1.3 The Work Function

In order to trigger gas breakdown and generate a plasma near the cathode, it is necessary for the cathode temperature to be high enough to emit electrons. Electron emission due to temperature, or thermionic emission, is governed by the Richardson-Dushman equation [4], which states that

$$j = AT^2 \exp\left(\frac{-e\phi}{k_{\mathrm{B}}T}\right) \tag{1.3.1}$$

where j is current density, T the temperature of the emitter in Kelvin, e the charge of an electron, ϕ the work function of the emitter, k_{B} the Boltzmann constant, and A a constant based on material properties. The emitter's temperature depends on both current density and the value of the work function of the emitter. The work function is a measurement of the amount of energy required to remove an electron from a material surface; the lower the work function, the less energy is needed. It is the only parameter that controls operating temperature for a given current density. Figure 1.1 illustrates the limitations that the work function places on material selection in cathodes. The Electric Propulsion and Plasma Dynamics Laboratory (EPPDyL) at Princeton operates a lithium Lorentz-force accelerator (LiLFA), a kind of MPD thruster. This thruster draws a maximum of 1000 A during operation. The cross-sectional area of its cathode is marked as the blue line on Figure 1.1. The

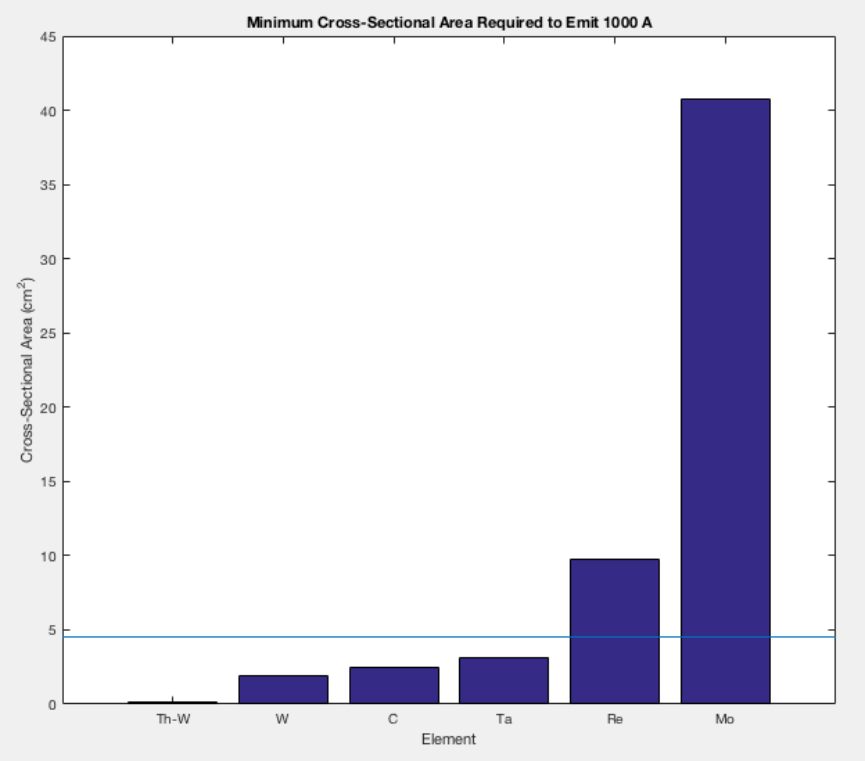

Figure 1.1: A plot of the minimum cross-sectional area needed to emit 1000 A of current without melting for various refractory materials. The blue line represents the cross-sectional area of the LiLFA.

area is computed using Equation 1.3.1 at the melting point of each material. The figure shows that there are only a few materials capable of handling the worst-case current density requirements in a size comparable to that of the LiLFA — namely tungsten, thoriated tungsten, carbon, and tantalum. Other refractory metals are included here, but their lower melting temperatures and higher work functions require a much larger cathode. In short, the work function is the biggest limiting factor in determining practical cathode lifespan.

1.4 Orificed Cathodes

One way around the cathode life issue is to use what is known as an orificed hollow cathode, as shown in Figure 1.2.

The cathode consists of a hollow cylinder with a narrow orifice at one end. Just inside the cathode from the orifice is an insert of a lower-work-function material. The propellant flows through the cathode and is ionized by electrons emitted by the insert; it then passes through the orifice and out of the cathode.

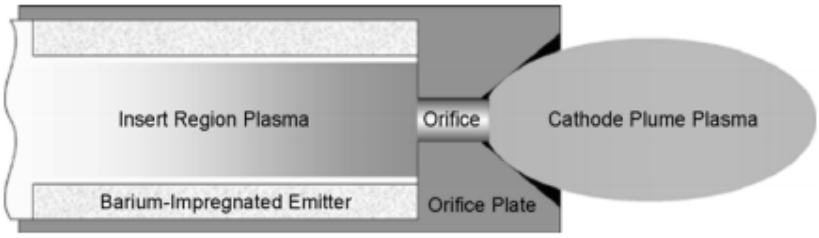

Figure 1.2: General schematic of a hollow cathode in operation. [4]

A hollow cathode is more efficient than a solid one, as the interior cavity confines primary electrons such that their energy goes into the plasma and not radiated out into free space. An orificed hollow cathode builds on this by blocking the exit down to a very small throat; in doing so, it prevents the low-work-function material from leaving the inside of the cathode and increases the plasma pressure inside the cathode. This is important both for insert life as well as cathode lifespan.

Furthermore, the orifice provides a reinforcing mechanism of resistive heat generation that allows for reliable steady-state operation. The low work function insert needs to be kept at thermionic emission temperature in order to sustain the plasma, which requires heat flow into the system. Depending on the orifice geometry, insert heating can happen in various ways. The three main methods are orifice heating, ion bombardment, and electron bombardment. Orifice heating occurs when a narrow orifice creates a large electric field and a high plasma density inside; this creates a high energy density, which delivers heat to the walls of the orifice. The heat is then conducted to the insert. Ion and electron bombardment both involve high-energy particles colliding directly with the insert, transferring energy kinetically. As orifice heating is an indirect heating method, the insert is spared some bombardment and therefore lasts longer.

The low work function material can be one of two types — a dispenser or a bulk emitter. Dispensers are pieces of a metal, usually tungsten, that have been impregnated with a combination of elements to significantly lower their work functions. They have very low work functions (approximately 1.5 eV) and as a result operate at very low temperatures (approximately 1200 °C). [4] Bulk emitters are similar to dispensers, except that they are made entirely of one material. Generally, their work functions are slightly higher and thus operate at a hotter temperature, but they have several advantages over dispensers; namely, they can handle more current for longer than a bulk emitter can, and ablation of bulk material does not lead to a reduction in the emitter's current carrying capability. As the material is uniform through its

entire thickness, ablation leads to exposure of more material surface area, while bulk dispensers can see loss of capacity due to the impregnated layer being ablated.

The relative simplicity of the orificed hollow cathode, combined with the temperature-lowering properties of the emitter, are both promising in terms of reducing cathode temperature and thus extending cathode life.

1.5 Prior Work

The only prior test of an orificed hollow cathode MPD thruster (OHC-MPDT) was by Mantenieks and Myers. [11] They used a tungsten cathode with a barium-calcium-aluminum insert in a tungsten matrix, as BaO-W inserts have been proven in flown spacecraft missions. In order to test different geometries, they used a sequence of four orifice plates that were press-fit on the end of the cylindrical cathode. Of these four cathodes, two created plasmas and generated non-trivial amounts of thrust.

Unfortunately, there were a number of problems with the experiment. First, none of the orifice plates would stay on during the test. One dislodged and melted to the anode, and the rest were removed due to poor fit. Second, inserts are highly sensitive to certain gases, such as oxygen or water vapor, which render them unable to emit electrons. In order to ensure that they function properly, dispenser inserts are usually kept in sealed containers and baked before use to remove any impurities. This experiment did not, however: "For these tests... special handling of the inserts was not possible during the assembly and testing of the cathode." [11] In short, the conduct of this experiment left much to be desired and leaves much room for exploration of the OHC-MPDT concept.

1.6 Research Objective

The goal, then, of this thesis is to further investigate the feasibility of the OHC-MPDT concept by designing, fabricating, and testing an OHC for an applied-field MPDT. As the promise of OHCs lies in their increase of cathode life, testing will require a quantifiable way to represent cathode life. This will take place through a simple before-and-after mass measurement — as the modes of cathode consumption remove material, a measurement of the change in mass provides a simple way to estimate the cathode consumption rate for an OHC in an MPDT. This thesis will proceed by detailing the design process of an OHC, justifying each decision, from material

choices to emitters to the surrounding thruster needed to test it. Next, the thruster will be modeled to ensure static and thermal stability during operation. Lastly, it will be tested, and the results analyzed to see whether a graphite OHC is a promising, life-enhancing concept for MPDTs.

Chapter 2

Cathode Design Process

Now that the motivation for an orificed hollow cathode has been established, this section describes the design of the cathode. First, a list of the constraints and parameters that guide successful cathode design is presented. Next, the cathode design is described, including material selection, orifice sizing, and gas flow concerns. The emitter is described, then the lack of a keeper and heater are all justified. The design process of the rest of the thruster needed to test the cathode is then detailed, and the assembly is considered as a whole.

2.1 Design Parameters & Constraints

Given what has been previously said about orificed hollow cathodes, and given the current experimental setup, there are several design constraints that need to be taken into account.

- The geometry of the new thruster should match that of the existing LiLFA as closely as possible. This ensures that performance measurements from the new cathode will be comparable to previously gathered data.
- The cathode should operate in a specified mass flow rate and current regime without melting. Historically, the LiLFA, a 30 kW thruster, has operated at no higher than 1000 A. The mass flow rate target for lithium ranged between 8 and 20 mg/s. Due to the increase in background pressure that gaseous propellants provide, the mass flow rate target for argon must be lower. Constraints on the pumps that operate the vacuum tank suggested that a mass flow rate of no more than 5 mg/s would be acceptable. Thus, the cathode should be able to

withstand 1000 A of current and 5 mg/s of gas flow without melting or becoming inoperable.

- The cathode should be able to form a tight gas seal with steel against vacuum, as any leak, no matter how small, could have deleterious effects on the thruster's ability to function.
- The cathode should be simple, requiring a minimum of material, complicated manufacturing techniques, and fabrication time in order to complete.

Other factors obviously do enter into the design process, but these four were the ones optimized for.

2.2 Cathode Design

The cathode was designed to match the dimensions of the LiLFA's cathode, designed and built by the Moscow Aviation Institute (MAI) in 1998. The previous cathode was a multi-channel hollow cathode, as shown in Figure 2.1. Liquid lithium flows into the cathode through the side-mounted pipe (4 in the figure), and then flows past an electrically and physically insulated heater (5), which evaporates it. The gas then flows out through the gaps between the tungsten pins (10), where it is ionized into a plasma.

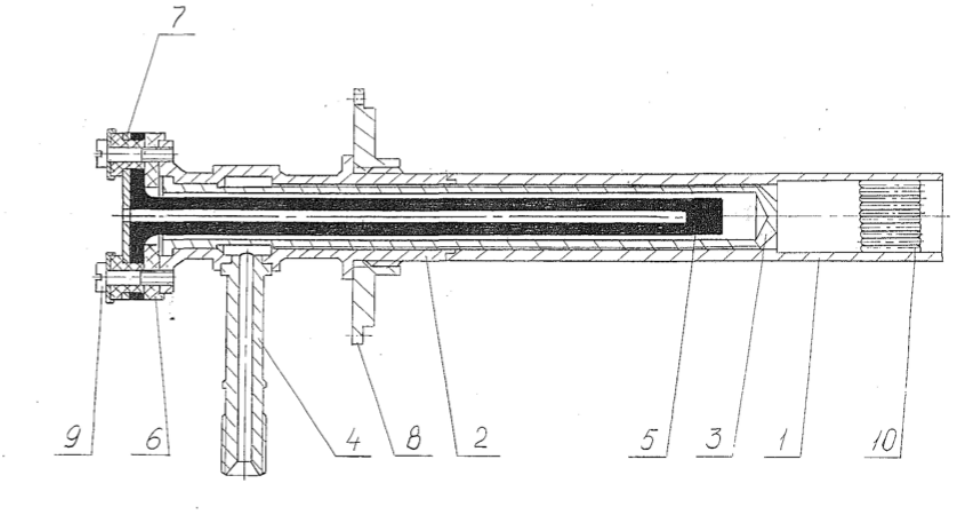

Figure 2.1: The LiLFA's multichannel hollow cathode. [7]

2.2.1 Material Selection

The cathode needs to maintain structural integrity while withstanding temperatures of over 3500 °C during operation. There are very few materials that remain solid with reasonable mechanical properties in this regime, and even fewer that are not impossible to manufacture without expensive tools. Of all the various refractory materials investigated, the Richardson-Dushman equation predicts that only tantalum, tungsten and graphite will survive at the desired current and cathode diameter. As such, materials considered for the cathode included graphite, tungsten, and tungsten-impregnated derivatives, such as thoriated tungsten. Tantalum was not considered due to its high cost, especially given that other materials performed better for less cost. Tungsten, or thoriated tungsten, is the traditional choice for a cathode material, as its melting point is the highest of all pure metals at 3695 K. [10] Furthermore, it is chemically inert with a number of other substances. However, it suffers from fatigue due to thermal stress, and eventually degrades over time. Furthermore, it is expensive, and requires heating and exotic cutting fluids in order to machine properly.

Graphite is an excellent alternative to tungsten. Its sublimation point is slightly higher than the melting point of tungsten, at 3923 K [10], and its electrical conductivity, while lower than that of refractory metals, is still quite high. A direct comparison is difficult due to graphite's anisotropy, but parallel to its layers its conductivity is 330 kS/m, which is comparable to tungsten at 189 kS/m [1]. Even better, graphite is relatively easy to machine, comparatively cheap, and easy to acquire at a high purity. Its main drawbacks lie in the relative ease with which it forms intercalation compounds with other materials under high temperatures. However, as it is known that pyrolytic graphite, a form of nonisotropic, semicrystalline graphite, will not interact strongly with emitter materials under certain cathode regimes [14], this was thought not to be a serious enough drawback to prevent the use of graphite for the cathode. As such, POCO AXM-5Q graphite was selected as the material of choice for the cathode due to its uniform, fine grain size and high purity.

2.2.2 Emitter

The emitter is the most critical part of the cathode, as it is what helps keep temperatures down to allow steady-state operation in a regime that does not melt the cathode. There are three major types of emitters: oxide deposits, bulk emitters, and dispensers. As mentioned in Chapter 1, oxide deposits and dispensers are generally better than bulk emitters at lowering operating temperatures at steady-state;

the best dispenser materials can get operating temperatures below 1000 °C at work functions lower than 2 eV. [4] However, they are much more prone to poisoning than bulk emitters, and especially in the case of oxide deposits, any form of sputtering can cause loss of active material, thus reducing the effective electron emission from the insert. Dispensers solve that problem by impregnation rather than surface deposits, but the poisoning issue remains, and is compounded by propellant issues. If the propellant gas is not pure enough (5 ppm is an approximate upper limit on impurities [4]), dispenser inserts can suffer from migration and deposition issues that reduce the amount of low-work-function material exposed to the plasma.

As such, the new cathode is specified to work with a bulk emitter. The bulk emitter chosen is lanthanum hexaboride, or LaB_6. LaB_6 has a long history of use as a cathode for spacecraft components, and is somewhat easy to acquire. While its work function is slightly higher than the BaO insert considered, at 2.67 eV [8], it still lowers the work function by more than 1.3 eV compared to graphite. Furthermore, due to the way the insert is ablated from the inside out, the rate of loss of LaB_6 slows as time goes on. This, combined with the lack of chemical reactions occuring at high temperatures, provides a longer working life at all current densities compared to a dispenser insert.

The insert (shown in Figure 2.2) slides into the hollow cathode from the rear. It rests right behind the orifice, as shown in Figure 2.9. Electrical and thermal contact are ensured by tolerancing the inner diameter of the cathode to be very close to the diameter of the insert.

2.2.3 Geometry

While the new cathode has an entirely different internal geometry, the external geometry was kept as close as possible to that of the MAI cathode. Because argon is a gas at room temperatures, heating the new cathode was deemed unnecessary. As such, modifications were made to the original internal geometry to simplify the cathode and implement the orifice.

The internal geometry was determined by several relevant factors. As there was no longer a need for a heater inside the cathode, the complex side-port propellant feed was discarded in favor of an axial feed. The inner diameter was set to match the outer diameter of the emitter, which the lab had acquired prior to its application in this cathode. Cathode length was determined by the geometry of the anode as well as the previous anode. The length was set to match that of the existing anode/cathode pair,

Figure 2.2: The lanthanum hexaboride insert used in the cathode.

which allows for comparison between old and new thrust measurements. Figure 2.9 shows the cathode and anode relative to each other.

The specification of the size and length of the orifice of the cathode was a critical component of the design process. Goebel and Katz [4] classify orifices into three different categories, which they label types A, B, and C. Type A hollow cathodes have a very narrow orifice that is much longer than it is wide; type B hollow cathodes have orifices that are at least as wide as they are long, if not longer; and type C hollow cathodes have an orifice that is almost, if not entirely, as wide as the inner diameter of the cathode itself. Depending on the type of orifice, different heating regimes dominate. Type A orifices produce resistive heating within the plasma, generating heat which disperses to the orifice plate and then to the insert. Type C orifices heat the insert through ion bombardment, as there is no restriction in the path of the ions traveling from anode to cathode. Type B orifices heat the insert through a combination of the two.

Part of the rationale for using an orificed cathode is to ensure long life of the insert material. A narrower orifice ensures that the insert material remains inside the

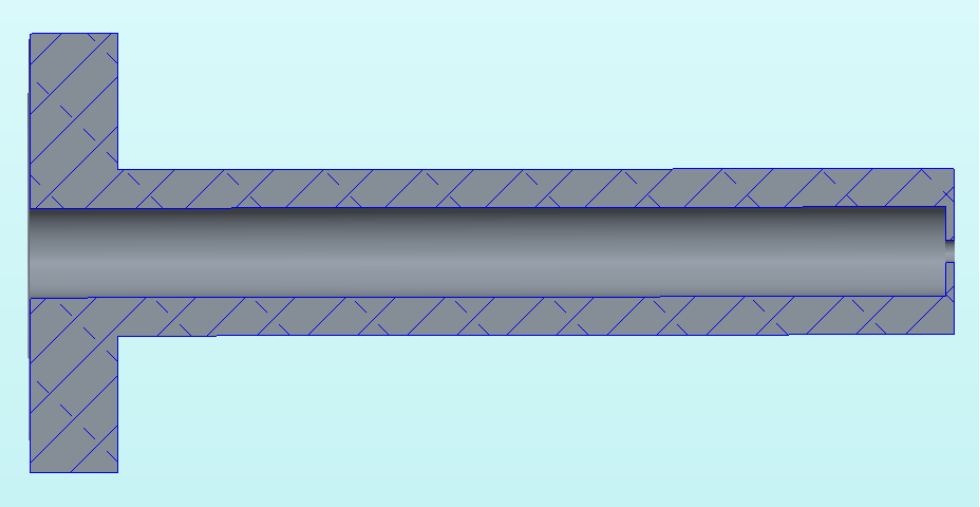

Figure 2.3: The new orificed hollow cathode.

cathode, rather than downstream. While the plasma pressure inside the cathode is higher with a narrow orifice, and thus there are more bombardments of the insert, it is harder for sputtered ions of the insert material to escape and be lost. Furthermore, the main heat delivery system for an insert in a cathode with a narrow orifice is indirect — ion bombardment stops being the primary heating mechanism, further extending the life of the cathode. As such, a narrow orifice is better for insert life. The higher plasma pressure inside the cathode created by a narrow orifice also aids in startup operation, by ensuring a density high enough to propagate breakdown and keep operating voltages low at low mass flow rates. However, an orifice that is too narrow will make startup nearly impossible, by preventing the electric field generated by the anode from penetrating inside the cathode with much strength. Furthermore, a too-narrow orifice will cause choked flow in the orifice at lower exit velocities than a larger orifice.

Most existing hollow cathodes operate at internal gas pressures between 1 and 10 torr [4], which ensures enough gas to reliably induce breakdown. Therefore, the orifice diameter needs to be chosen to make sure that the steady-state operating pressure inside the cathode is between 1 and 10 torr. To do so, the gas flow through the orifice can be modeled using simple Poiseuille flow modified for compressible flow. It can be easily shown that the rate of gas flow through a pipe can be given by

$$N_m = \frac{\pi}{16\zeta}\frac{a^4}{l}\frac{{P_1}^2 - {P_2}^2}{R_0 T}[4] \tag{2.2.1}$$

where N_m is the mass flow rate in mol/s, l is the length of the pipe, a is the radius of

the pipe, P_1 is the upstream pressure, P_2 is the downstream pressure, ζ is the viscosity, R_0 is the universal gas constant, and T is the temperature. Solving Equation 2.2.1 for the volumetric flow rate Q and rewriting in terms of P_1, we find that

$$P_1 = \sqrt{{P_2}^2 + \frac{0.78 Q \zeta T_r l}{d^4}} [4] \tag{2.2.2}$$

where $T_r = T/T_m$ and d is the diameter of the orifice. Assuming further that P_2 is approximately zero, Equation 2.2.2 yields an expression for internal pressure in terms of the diameter and length of the orifice. As shortening the orifice length increases external electric field penetration, and thus thruster performance, taking l equal to 0.05" yields a potential range of orifice sizes from 0.111" (at 10 torr) to 0.352" (at 1 torr). Thus, we decided on the next largest fractional size up from 0.111", which was 0.125", as the orifice size. This provides a cathode pressure of 7.922 torr, which provides a lower discharge voltage.

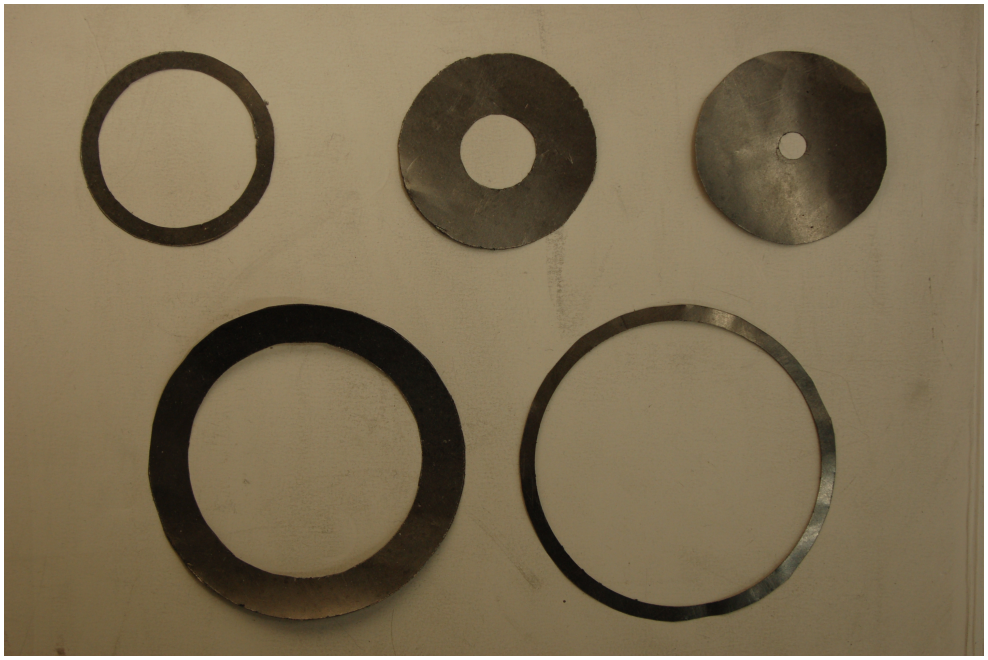

Figure 2.4: The five graphite seals made out of Grafoil in order to prevent gas leaks from occurring.

In order to avoid gas leaks, which add uncertainty to the measured gas flow rate and may cause electrical shorts, it was necessary to seal the interface between the cathode and the gas supply tubing. To reduce the number of mechanical connections to the graphite of the cathode, this interface also served as the current source. It was necessary to find an electrically conductive, compressible material that would

hold gas pressure against vacuum, that did not outgas in vacuum, and that wouldn't melt at operating temperatures. A type of flake graphite called Grafoil was used to make the seals themselves, as shown in Figure 2.4, which were compressed between the cathode and gas supply. Grafoil was also used as a seal between the cathode and insulation, as well as the anode power supply and the insulation, to make doubly sure that no gas could get by.

2.2.4 Keeper and Heater

Despite most hollow cathodes having both a keeper and a heater, it was decided that the cathode would have neither. Both keepers and heaters are ways of pre-heating the insert so that the thruster begins operation at steady-state temperature, which prevents arc attachment to the cathode body, lengthening cathode life. A keeper is an electrode that sits between the cathode and the anode that is used to initiate cathode discharge and bring the cathode up to temperature before full discharge is obtained. A heater is a resistive device that transfers heat by conduction to the cathode to ensure that the insert remains in the emitting regime.

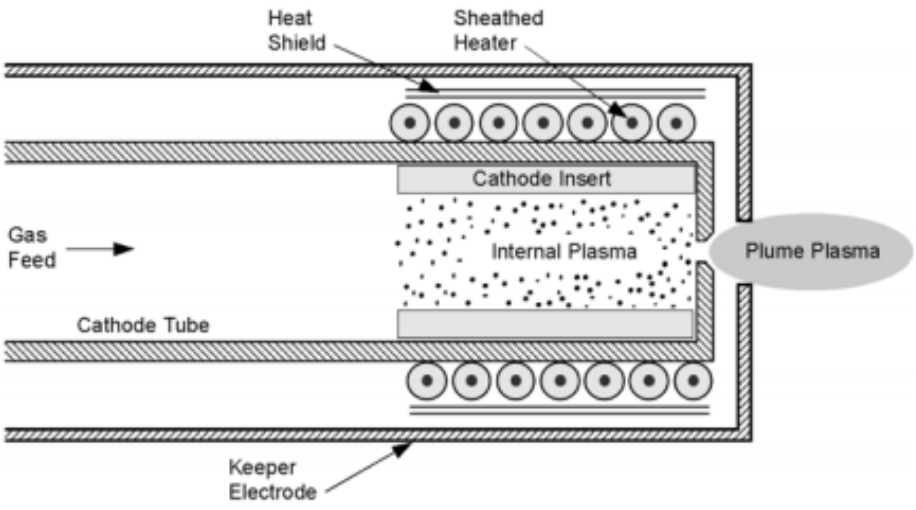

Figure 2.5: A diagram of a hollow cathode with insert, heater, and keeper. The heater heats the insert, while the keeper provides cathode protection. [4]

The argument against a heater was based on practicality. A heater in contact with the outside of the cathode would be exposed to the plasma, and thus might potentially become a location for arcing if it could not be tied to cathode potential somehow. A heater in contact with the inside of the cathode would complicate the

cathode geometry severely. As the heater should not come in contact with the gas, the hollow cathode would have to have a separate chamber for the heater, similar to the LiLFA's cathode (see Figure 2.1). This would mean, however, that an axial gas feed would no longer be practical, and that would significantly complicate the design to the point of making it unfeasible. Ultimately, the idea of using a heater was shelved for simplicity's sake.

A keeper, on the other hand, is a much more critical part of a hollow cathode. As illustrated in Figure 2.5, the keeper sits outside the cathode, between it and the anode. It serves several roles beyond pre-heating the cathode; it also provides a method to keep the cathode hot if power to the anode is somehow interrupted, and it protects the cathode orifice plate from bombardment by ions attracted to the cathode that might cause sputtering and destruction of the orifice. As such, it is a life-extending component. The addition of a keeper to the new thruster's cathode, however, would require running a current carrier through two differently-charged plates without making electrical contact and in such a way that prevented gas from flowing through the insulator at 2000°C. As this is a significant engineering challenge replete with complications, and because laboratory work requires an operating time on the order of 100 hours instead of the 10,000 hours required for space qualification, we opted for a simpler design.

2.3 Anode Design

Due to concerns that operation with argon gas would result in higher operation temps that could damage the tungsten LiLFA anode, a graphite anode was built for the purposes of the proof of concept of the OHC-MPDT design. The new anode is also made of graphite for much the same reasons as the cathode — ease of manufacture, low cost, high electrical conductivity, high melting point. Otherwise, its geometry is almost identical to that of the new thruster. As shown in Figures 2.6 and 2.7, the anode matches that of the LiLFA quite closely. The interior of the anode follows a conventional converging-diverging nozzle, with the contour of the diverging section following the magnetic field lines of the solenoid as given by the Biot-Savart law. It is held in place using a lockring, which clamps a flange down onto the large plate that delivers the current to the anode.

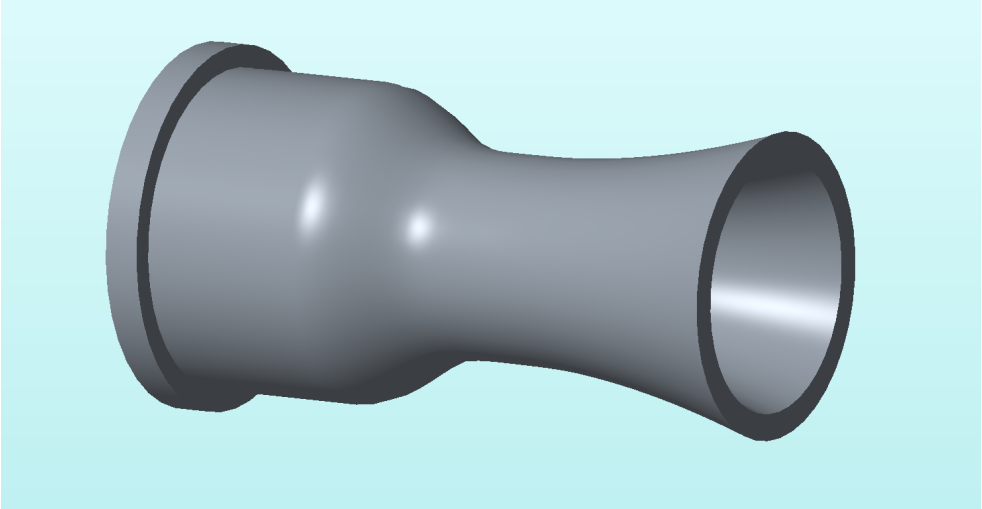

Figure 2.6: A CAD rendering of the anode built for testing the graphite OHC.

2.4 Final Thruster Design

Two large steel plates provide attachment points for the cathode and anode, as well as ample surface area for clamping and electrical feed attachment points. The plates are made of Rolled Alloys' RA 253-MA alloy, a chromium-nickel steel alloy with cerium, manganese, nitrogen, carbon and other trace elements added. This alloy is one of the most resistant to deformation under heat available, and is resistant to oxidation above 1000°C [2]. The plate in contact with the cathode (henceforth referred to as the cathode plate) has a slightly recessed hole in the center to allow positive alignment of the cathode. The cathode plate is held to the anode plate by screws held by ceramic spacers in order to ensure electrical insulation. It has a hole in the center for gas flow into the cathode; a 1/4" tube is welded to the back to provide a mounting point for the gas feed tube.

The anode is held onto the anode plate by a ring with a chamfer to grab the flange on the anode,as shown in Figure 2.11. It is also made of RA 253-MA for its heat-resistant properties. As this ring will be in contact with the anode, it will get quite hot, and thus needs to be able to withstand high temperatures without losing strength or deforming. The use of a ring takes advantage of graphite's compressive strength, allowing a large clamping force without risk of cracking the anode.

Furthermore, there needed to be something physically separating the anode plate and cathode that would provide alignment, sealing against errant gas, and insulation. The cathode-anode separator is shown in Figure 2.12. As the potential difference between the anode and cathode could be as high as 1 kV in the startup procedure,

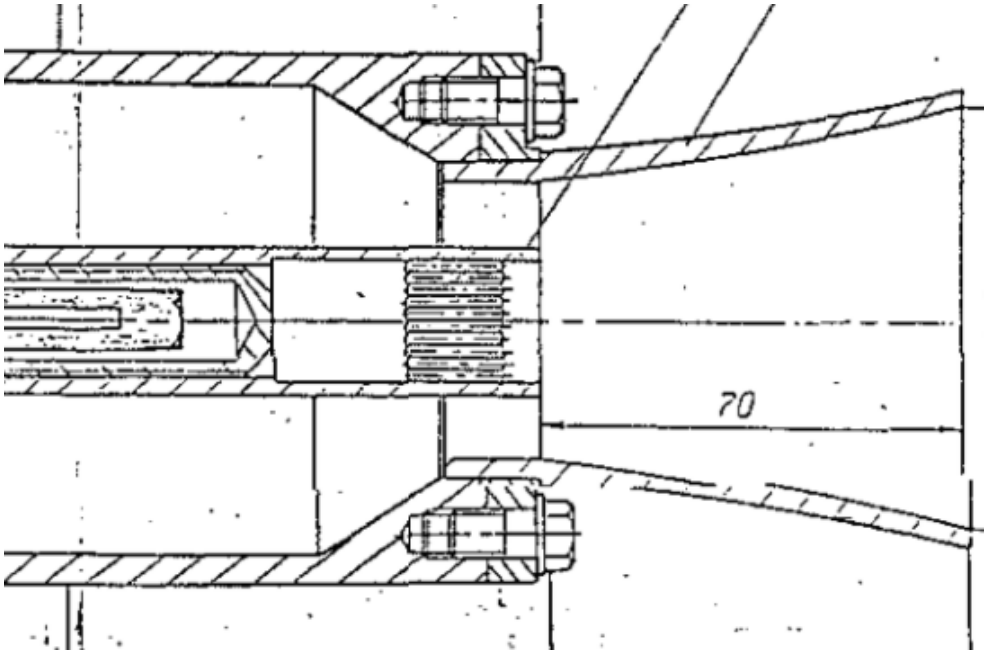

Figure 2.7: The LiLFA's anode and cathode - note how the anode curves with the magnetic field lines.

the material needs to have an enormous resistivity to prevent current flow. Ultimately, boron nitride was chosen to make the spacer between cathode and anode plate, as it has much the same properties as graphite (easy to machine, relatively low cost, extremely high melting point, retains strength at high temperatures) except that it is electrically insulative.

Engineering drawings of each part are provided in Appendix A.

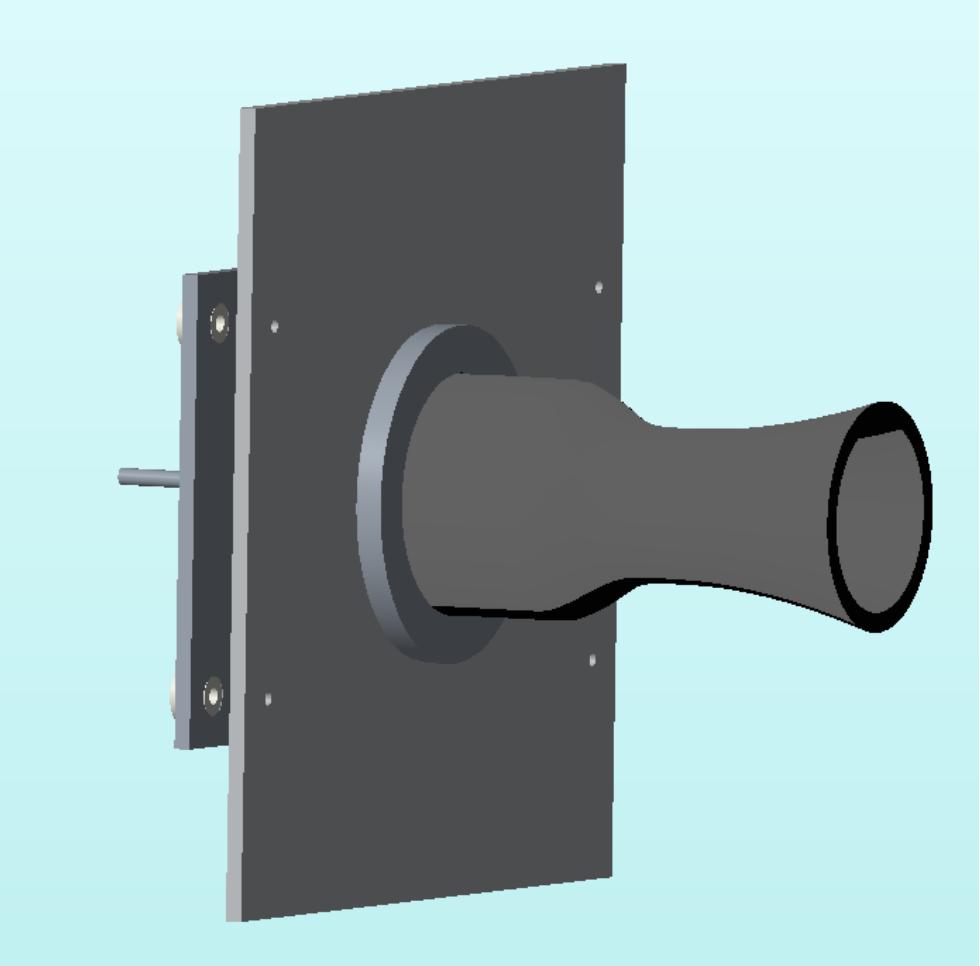

Figure 2.8: A CAD rendering of the thruster assembly build for testing the graphite OHC.

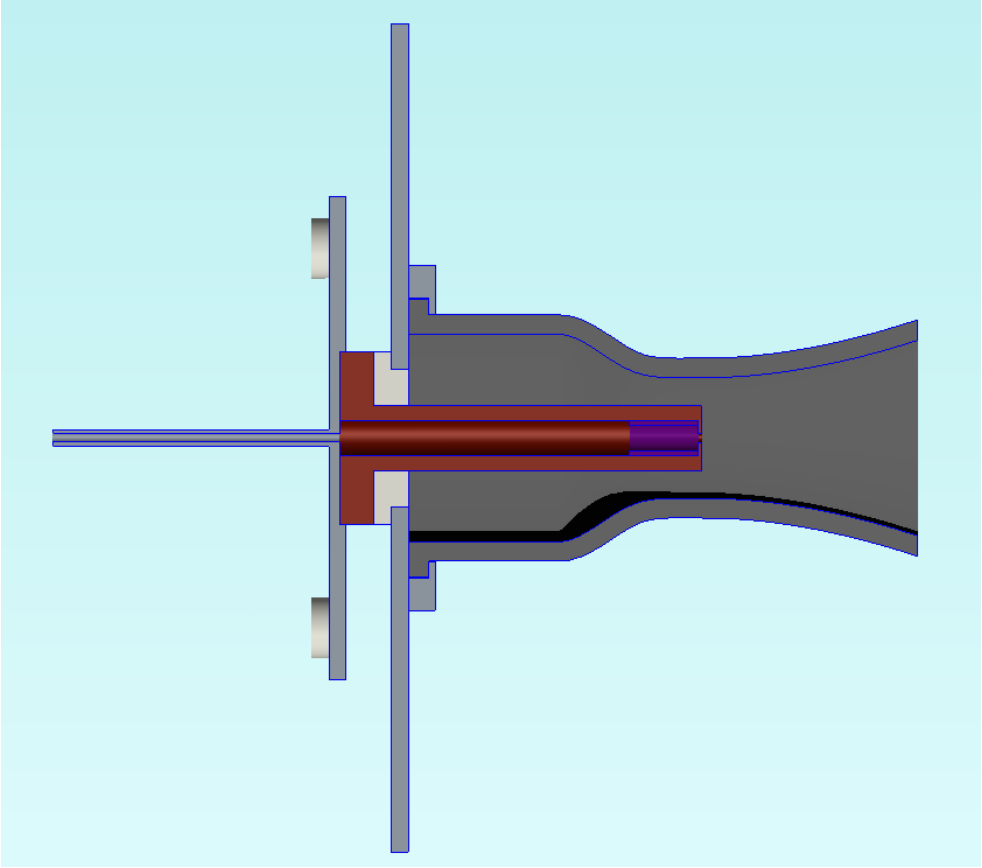

Figure 2.9: A cutaway view of the thruster assembly. The anode is dark grey, the lock ring, anode, and cathode plates are light grey, insulators are white, the insert is purple, and the cathode is dark orange.

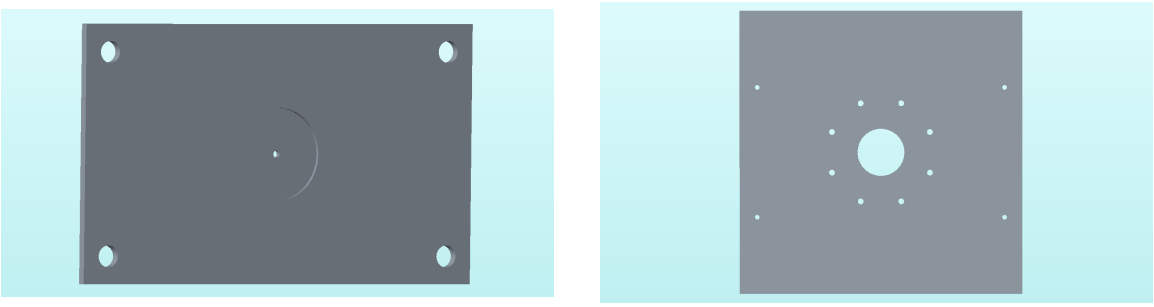

Figure 2.10: The plates for carrying current to the cathode (left) and from the anode (right).

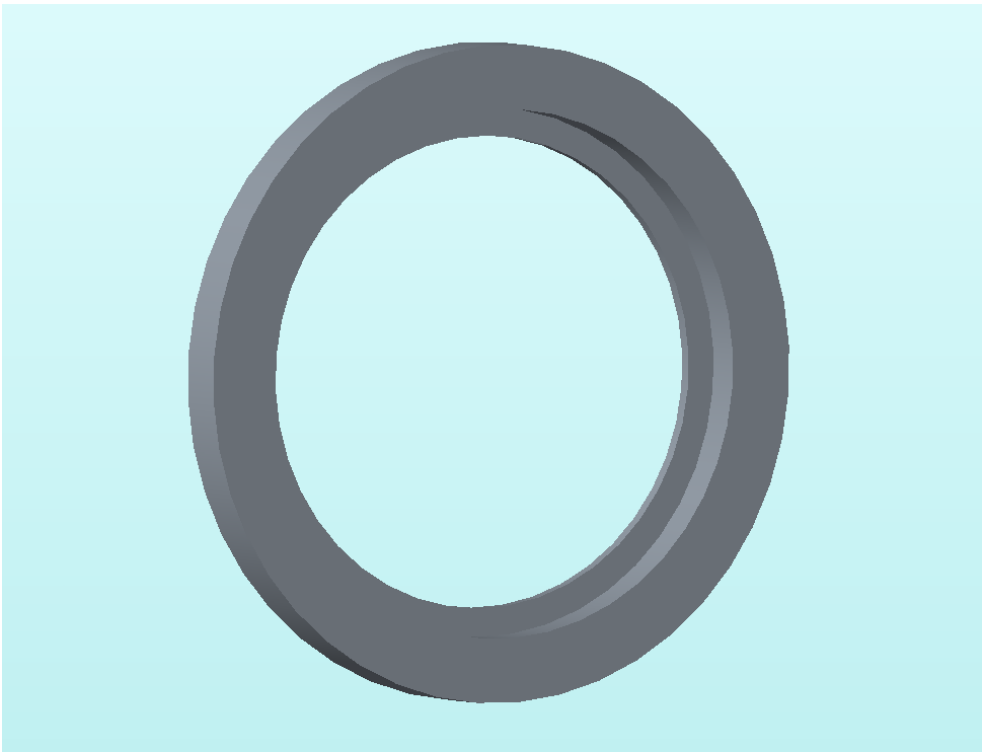

Figure 2.11: A CAD rendering of the compression ring.

Figure 2.12: A CAD rendering of the cathode-anode separator.

Chapter 3

Static and Thermal Modeling

In order to ensure compatibility of the orificed graphite cathode with the thruster setup, as well as the integrity of the new thruster assembly, it was necessary to build a model in COMSOL to ensure that thermal and mechanical failure would not be an issue. As components for the cathode and other parts were very expensive and procuring them took several months, failure was not an option. Thus, modeling was done in COMSOL Multiphysics to ensure the robustness of the proposed design under thermal and static load.

3.1 Stress Modeling

The two main worries behind the stress modeling involved graphite. Graphite is a brittle material that is good in compression and little else. While the compressive strength of the grade of graphite selected for this project is approximately 138 MPa, its tensile strength is only about 62 MPa, and its strength in shear, while not often tabulated, is quite low. Graphite's comparatively poor behavior in shear and tension led to worries of cathode and especially anode failure due to the force of gravity causing a torque, machining forces, or accidental forces applied during installation. As the edge of the lock ring applies a shear stress in the graphite flange of the anode, it was necessary to determine the magnitude of the force that the graphite could withstand without cracking.

Also, the lockring and graphite themselves had a restriction in thickness. The solenoid sits very close to the anode plate and lockring during operation; there is no more than a half-inch of clearance between the two. As arcing is a serious concern,

the lockring and solenoid ideally would be as far away as possible from each other. However, the thinner the graphite underneath the lockring is made, the higher the shear stress in the corner and the more likely it is to fracture. As such, the goal was to both ensure that there was a healthy margin of safety in the flange region and to minimize the thickness of the anode lockring to ensure structural integrity and minimize the risk of arcing.

Lastly, the anode machining process places loads in the axial direction when cutting the exterior of the anode. Ensuring that the part is machinable was deemed an important caveat to consider before proceeding with the design. In order to do all these things, a COMSOL model was built of the thruster assembly. Finite element simulations were run on this model. In building the model, the following assumptions were made:

- All materials were isotropic. This reduced the need to specify material directions in complex geometry and simplified the solution of the problem immensely. To first order, it is a good approximation, as the blend of graphite used is approximately isotropic and the steel and boron nitride are perfectly so.

- Loads were applied only to the anode - the assumption being that the cathode would hold up fine under gravity, and the anode shields the cathode from any external loads in all except one direction. The anode will fail before the cathode will if a load is applied in an off-axial direction.

- To simulate the force of gravity, the anode volume was subjected to a body load (load on every point of the anode) equivalent to the force exerted on the anode mass by gravity. This load was applied in the -Z direction in the model, which corresponds to the direction of gravity relative to the installed thruster. The load due to a cutting tool was modeled as a line load on the top of the thruster, as illustrated in Figure 3.7. A point load was initially tried but found wanting, as it did not show forces in the joint between the anode and the lockring. Cutting forces are notoriously hard to model [15], so the limit was found by increasing the force until the anode hit its yield stress.

The built COMSOL model is shown in Figures 3.1 and 3.2.

A representative sample of von Mises stress results in the anode due to gravity is shown in Figs. 3.3 & 3.4. The model matches what would be expected. The highest-stress regions are at the joint of the anode flange with the anode wall, and the peak stress occurs at the point in the +Z direction, as would be expected if the body load

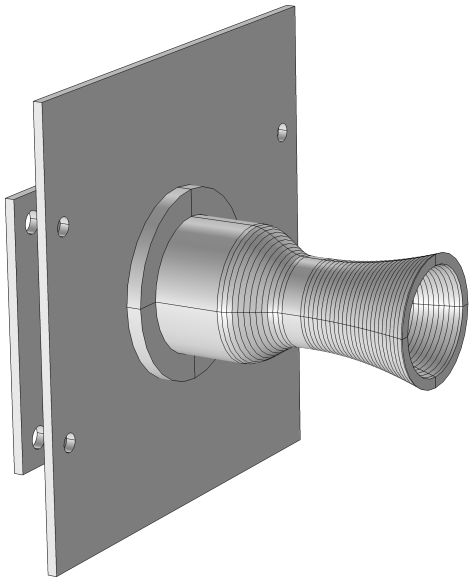

Figure 3.1: The COMSOL model of the thruster built for finite element analysis.

is applied in the -Z direction. The maximum von Mises stress is 69.184 kPa, which is several orders of magnitude smaller than our grade of graphite's tensile strength of 62 MPa [5]. As such, it is reasonable to conclude that the anode will not collapse under its own weight. The high-stress region can further be reduced by adding a chamfer at that corner. This was implemented on the actual anode.

Next, a point load was applied to simulate the machining process of the outside of the anode. It was applied at the tip, as that creates the largest cantilever and thus the largest shear stress in the graphite. Upon simulation, the point load applied at the tip of the anode created next to no change in stress in the flange of the anode, even at very high applied forces. This seemed slightly unphysical, so the load was instead modeled over a short line segment at the tip of the anode.

The high shear stress at the tip (shown in Fig. 3.7) was ignored, as that lies in material that would be cut away during a machining operation. As a result, the von

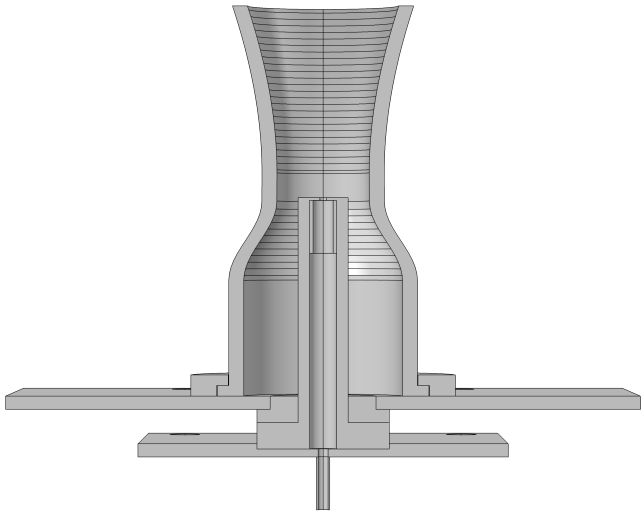

Figure 3.2: A cutaway of the COMSOL model, illustrating the internal geometry of the thruster.

Mises stress at the base was the only one taken into consideration. Ultimately, the line load required in order to create a von Mises stress equal to that of the yield criterion was approximately 3.5 kN; as this was well above any force the CNC machine would apply to the anode, the manufacturing process was determined to be feasible.

Once the manufacturing feasibility had been checked, it was necessary to do an optimization of the anode flange thickness to ensure the thruster would fit in the solenoid. Measurements taken on the solenoid indicated that a total space of 0.5" would be available; to start, the total thickness was taken to be 0.4". Running a series of finite element models, again with the gravity load, and varying the anode flange thickness and the lock ring flange thickness while keeping their sum constant generated Table 3.1.

It was expected that the values of the von Mises stress in the flange would increase

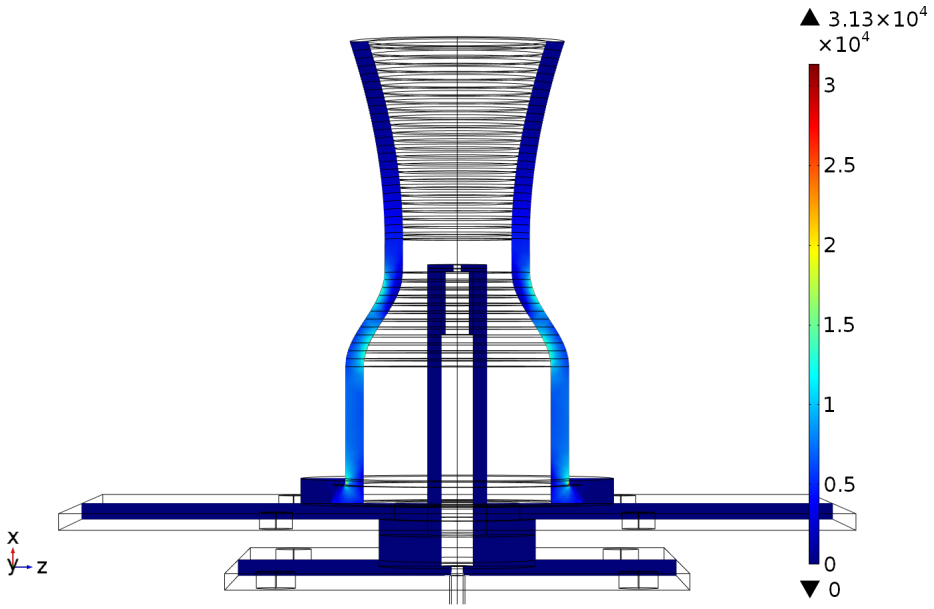

Figure 3.3: The results of applying a body load equal to the force of gravity to the anode.

Table 3.1: Maximum von Mises stress in the anode due to an applied body load with varying mesh size.

Anode thickness (in)	Max stress, normal mesh (kPa)	Max stress, finer mesh (kPa)
.1	72.899	60.978
.2	68.992	65.746
.25	131.128	70.291
.275	128.525	69.484
.3	78.018	69.184
.325	138.221	59.465
.35	96.525	57.727

as the thickness of the flange decreased; however, this did not occur. Instead, the values jumped, ranging from a low of 68 kPa to a high of 138 kPa. These results are not physical, as the stress should increase continuously as the thickness of the anode decreases. To better model the results, a finer mesh was generated and the process re-run, generating the second column. The results, again, are not particularly linear, but they seem to be converging around a narrow range of values. Therefore, the calculations were done by hand to see what the difference in moment would be at the flange given the variation in lock ring thickness. It was found that the moment varies very little, although thicker seemed to be better as intuition would suggest. Thus, the flange thickness was specified at 0.4", while the lock ring flange was specified at

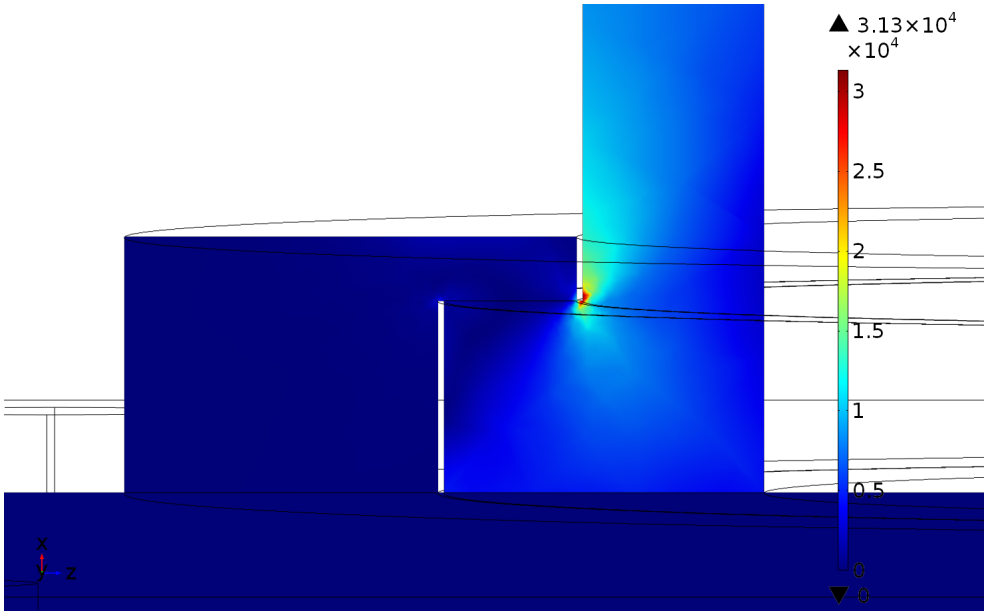

Figure 3.4: A close-up of the attachment point of Fig. 3.3, showing the von Mises stress maximum in the corner of the anode flange.

0.1". These values were chosen for their ease of machinability, as the steel of the lock ring would warp at small thicknesses due to the heat of cutting.

3.2 Thermal Modeling

The bigger question regarding the as-yet-unbuilt thruster involved heat transfer: would it melt at steady-state operating temperature? Intuitively, one would expect the cathode not to melt, as the whole point of the insert and orifice is to lower working temperatures so that the cathode does not melt. Evaluating the Richardson-Dushman equation with a work function equal to that of LaB_6 (2.67 eV) and a current density of 200 A/m^2, one gets a temperature of 1983°C. This is below the melting temperature of graphite, so the cathode and anode will not be damaged. However, the anode and cathode plates are not made of graphite, and thus might suffer from high temperatures. As the temperature at which they lose structural rigidity is much lower — only 1083°C [2]— heat transfer from the cathode and anode could cause them to melt or deform, significantly impacting the thruster's performance.

To verify that this would not happen, the same COMSOL model was used to solve the heat equation over the cathode, anode, cathode plate, and anode plate. The following assumptions were made in order to use the model:

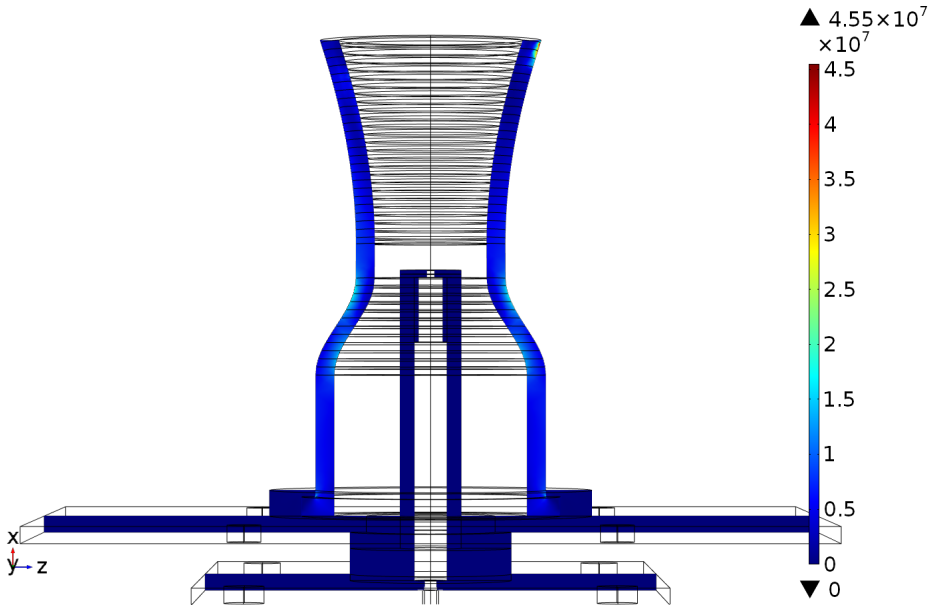

Figure 3.5: Overall results of application of an 800 N force to the last 1/4" of the anode.

- All materials were modelled using their standard properties, which came from CRC's Handbook [10], the material specifications of the graphite manufacturer [5], and various papers.

- As plasma heating is a major contributor to the heat flux into the cathode and anode, it makes sense to model the plasma. While COMSOL has a number of plasma-modeling tools, modeling the plasma in this case, with a number of unknown parameters that needed to be verified by experiment, was not a good idea. A plasma model could have been built, but it would not necessarily have been a good match with the physics going on in the thruster, and thus the idea was abandoned.

- Boundary conditions were enforced as well. The exterior of the anode was allowed to radiate to the atmosphere. The outer surfaces of the anode and cathode plates were also allowed to radiate, but the inner surfaces (the ones that faced each other) were not, as COMSOL is unable to model radiative energy transfer between surfaces. In order to try to model the temperature effects due to the plasma, a temperature gradient was enforced in the cathode, with the tip at 3500°C and the body varying as the results of the heat equation. This represents a worst-case scenario, with the tip of the cathode being heated to close to evaporation temperatures. The bottom of the anode plate was held

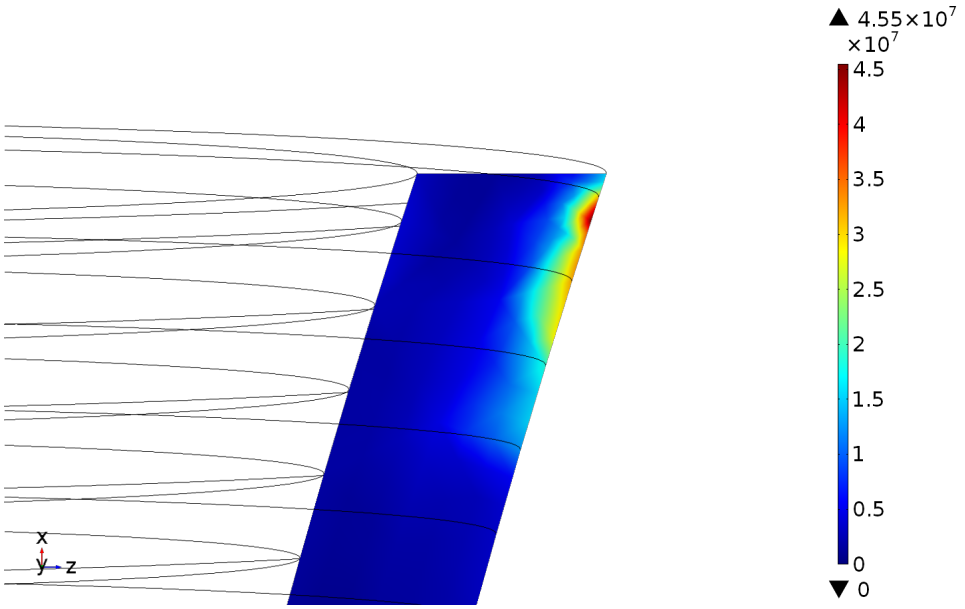

Figure 3.6: A close-up of the von Mises stress at the point of application of the line load, showing the maximum stress in the simulation.

at a constant 50°C, as it rests on a water-cooled plate.

- As the solution to the heat equation should have azimuthal symmetry in this case, the solution was only calculated on a quarter of the thruster in order to reduce computational time.

As seen above in Figure 3.8, the heat solution shows a maximum temperature at the tip of the cathode of 3500°C, as is expected. The maximum temperature in the anode plate is 893°C, while the maximum temperature in the cathode plate is almost the same at 889°C. As both of these values are below the point where RA-253MA loses structural rigidity (1083°C), and the creep failure rate at this temperature is still small, it is reasonable to assume that the anode and cathode plates would not lose their structural integrity or melt during steady-state operation.

Lastly, it was important to check that the steel feed line into the cathode would not heat up enough at its end to melt the Teflon hose that runs from the gas tank to the thruster. In order to do so, the length of the feed line was varied and the maximum temperature was recorded for each length, as shown in Table 3.2.

The melting point of Teflon is 599.8 K [3]. The table shows that the tip of the feed line is below that value at distances greater than 3 inches; as such, the feed line was made 5 inches long, to add in a safety factor.

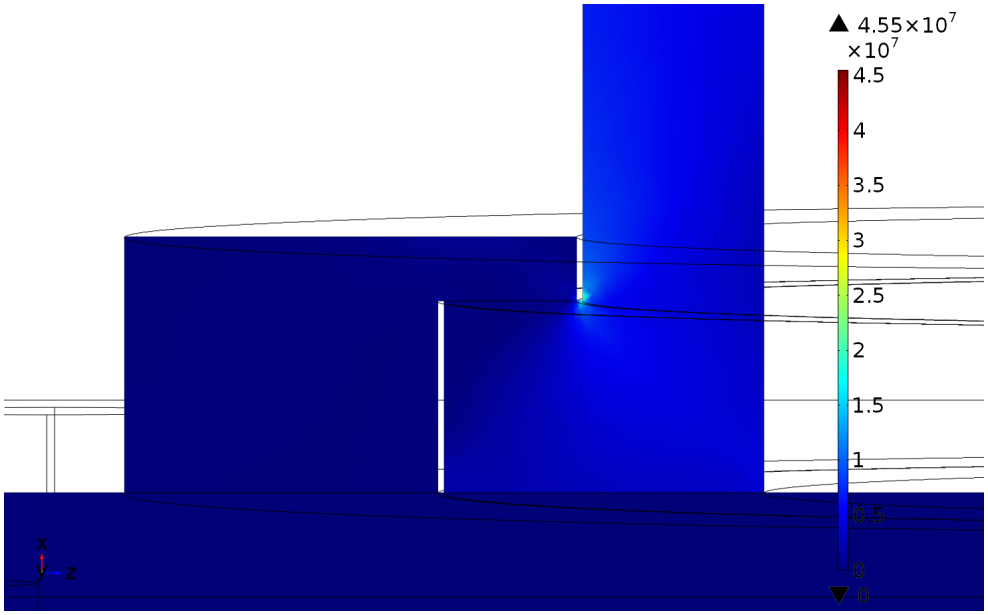

Figure 3.7: A close-up of the von Mises stress at the anode-lock ring interface. Maximum von Mises stress was approximately one-quarter that of the point of application, at about 10 MPa.

Table 3.2: Temperature at end of argon feed tube as a function of the length of the tube.

Length of tube (in)	Temp. at end of feed tube (K)
1	856.2
2	656.6
3	545.2
4	474.4

3.3 Summary

The new thruster was modeled thermally and statically to ensure the quality of the design. Using a finite element solver, it was shown that the anode was stable under its own weight and an applied force to simulate the cutting process. Thermally, the thruster apparatus was modeled to ensure that the plates holding the thruster up would not lose their structural integrity at worst-case scenario operating temperatures. Again, it was shown that the supporting plates would withstand operating temperatures. Optimizations were run to see what the maximum thickness that the anode flange could withstand was and to see how short it was possible to make the gas feed pipe to ensure the Teflon hookup would not melt.

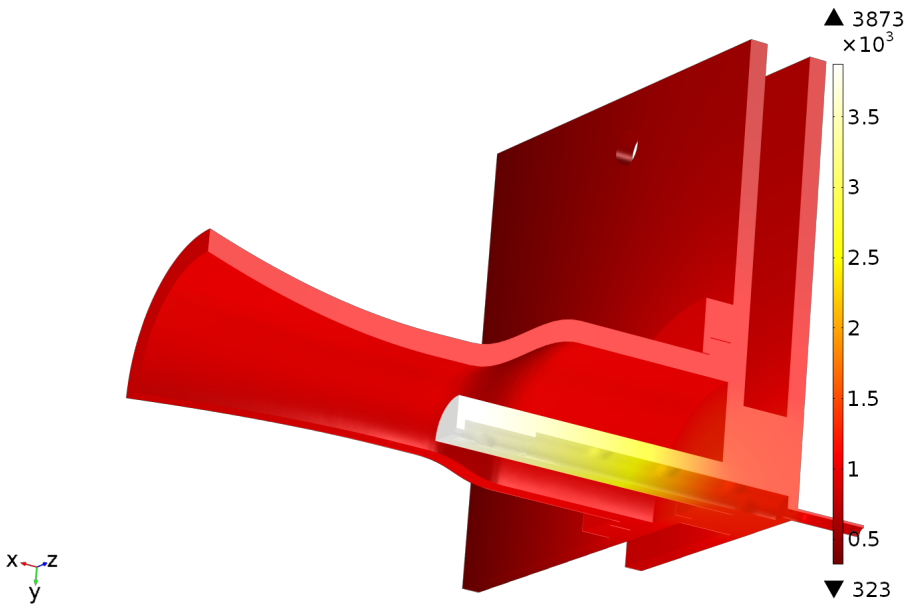

Figure 3.8: The results of applying the specified thermal load to the thruster assembly.

Chapter 4

Results & Discussion

Presented below are the results of the experiment, a discussion, and recommendations for future research.

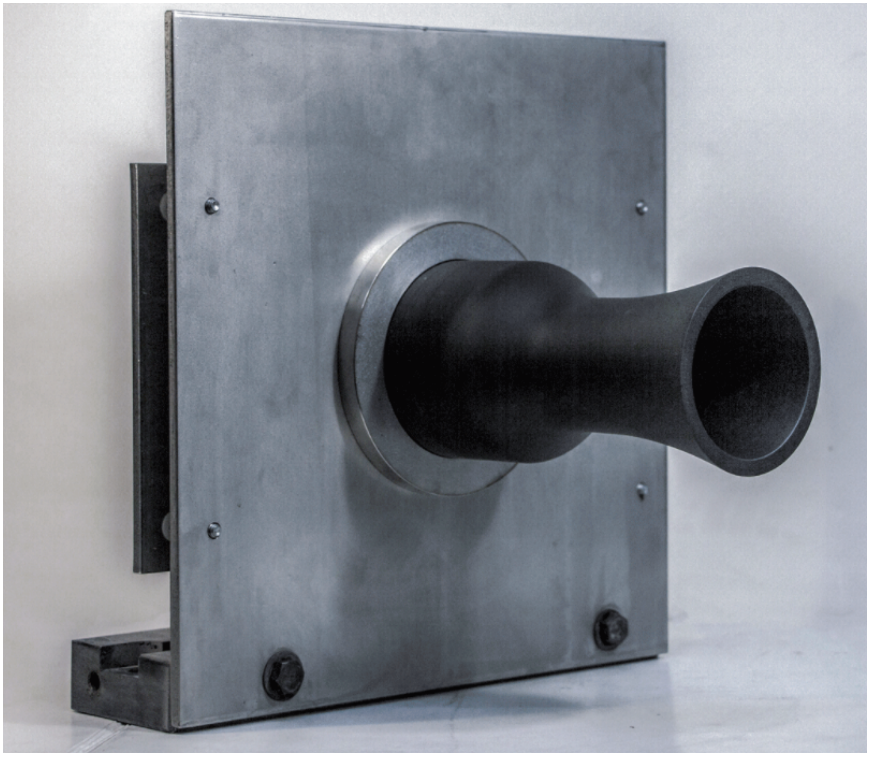

Figure 4.1: The completed thruster.

Figure 4.2: A side view of the completed thruster.

4.1 Thruster Testing & Results

Once the thruster was fabricated, assembled, and installed in the EPPDyL's MPD tank, it was fired to see how well the design worked. As the goal of the experiment was to measure the rate of consumption of a graphite OHC, it became necessary to determine a way of measuring that rate. The method of computation is very simple. If one knows the mass before and after a firing, and the amount of time for which the thruster operates, it is easy to compute an average rate of change. Therefore, we measured the masses of the thruster and insert before and after firing, and measured the amount of time for which the thruster was operational using a LabView data logger. From this information, we can back out the average time rate of change.

The experiment took place in one of the EPPDyL's vacuum chambers, a diagram of which is shown in Figure 4.3. The chamber is capable of pumping down (by the use of three pumps) to an ultimate vacuum of approximately $2\text{x}10^{-5}$ torr. The chamber is equipped with a high-current, high-voltage power supply that can deliver several kilowatts of power at a potential of 100 V. To start the thruster, however, a higher voltage is necessary to instigate breakdown. A separate, extremely high voltage power supply provides up to 1000 V in order to trigger breakdown. Before each experiment began, background pressure in the tank was about $5\text{x}10^{-5}$ torr; during operation, the pressure rose to no more than 10 milliTorr before the thruster was shut down.

The thruster was fired eleven times. The longest sustained operation lasted for 6 minutes; all the rest were under a minute long. A photograph of the plume of the

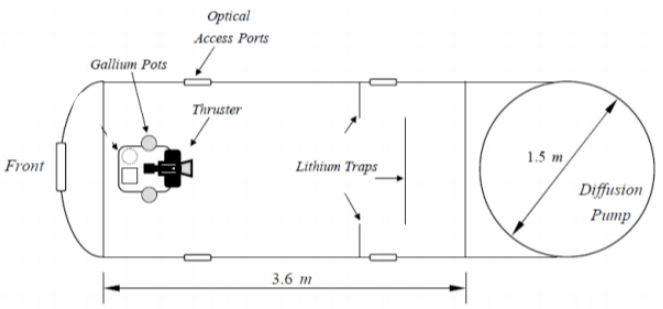

Figure 4.3: A diagram of the layout of the high vacuum facility at the EPPDyL. The gallium pots, while present, are not currently in use. [9]

longest operating period is shown in Figure 4.4. As evidenced by Figure 4.5, minor flares caused by gas leaks were present, indicating that the graphite seals were not perfect in sealing gas inside the cathode. As time went on, the average time of firing dropped, until after about 10 minutes of pulsed operation it ceased to light.

After the firing, the tank was opened, the cathode and insert were removed, and both were massed. Results from the massings are shown below in Table 4.1.

Table 4.1: Measurements of the mass of cathode components before and after firing.

	$t = 0$ sec	$t = 615$ sec
Cathode Mass (g)	157.733	157.638
LaB_6 Mass (g)	5.436	5.436
Combined Mass (g)	163.169	163.071

These values were used to calculate an average rate of cathode ablation. By consulting the raw data, the total time of operation was computed by addition of the time intervals during which more than 100 A of current was measured. (See Appendix B for Matlab code that did part of this.) Dividing the net change in mass by the total amount of firing time gives $(\frac{dm}{dt})_{\text{avg}}$, as shown in Table 4.2.

Table 4.2: Computation of the average rate of change of mass of the cathode.

Δm	.098 g
Δt	615.0 s
$(\frac{dm}{dt})_{avg}$	1.593E-4 g/s

A second round of testing was completed after it was discovered upon opening the tank that the insert had slid down the cathode (see Figure 4.6) and was not in

Figure 4.4: The thruster in operation. The bright streak in the plasma streaming out of the anode is a plume, which indicates attachment of the plasma at a point rather than diffuse attachment.

the correct place for proper cathode emission. The same testing procedures were followed the second time as the first. The thruster was reassembled with the insert in the correct place and the vacuum tank was pumped down again. The thruster was only fired three times over the course of the second test. Current density dropped compared to the previous round of tests, indicating that the emitter was, in fact, emitting as it should have. Results from the second round of firing are shown in Tables 4.3 & 4.4.

Table 4.3: Measurements of the mass of cathode components before after the second firing.

	$t = 0$ sec	$t = 328.3$ sec
Cathode Mass (g)	157.638	157.066
LaB_6 Mass (g)	5.436	5.433
Combined Mass (g)	163.071	162.500

It is not rigorous to compare the measurements between this test and the first test,

Figure 4.5: The slightly reddish plume of plasma directly above the anode is indication of a gas leak, as plasma should not be present outside of the confines of the magnetic nozzle during operation.

Table 4.4: Computation of the average rate of change of mass of the cathode for the second firing.

Δm	.572 g
Δt	328.3 s
$(\frac{dm}{dt})_{avg}$	1.745E-3 g/s

as both operated at different currents and voltages. As evaporation is a function of current density, the operating parameters will affect the erosion rate. Therefore, it is better to compare change in mass per unit power. Knowing that, for electric circuits, $P = IV$, it follows that

$$E = \int P dt = \int_{t_1}^{t_2} I(t)V(t)dt \approx \sum_{i=1}^{n} I(t_i)V(t_i)\Delta t \tag{4.1.1}$$

where Δt is the forward time step $(t_{i+1} - t_i)$. The measured current when the thruster was not operating was quite noisy due to the need to measure large amounts of current. This led to non-trivial power values computed by the LabView data logger

Figure 4.6: The incorrect location of the LaB_6 insert during initial firing of the thruster. It should have been at the other end of the cathode.

even when the thruster was not in operation, as the measured voltage was a more-or-less constant 70-80 V when the thruster was not operating. As such, a threshold of 20 A of measured current was used as the cutoff for operation. The results of these calculations are listed in Table 4.5. The code to compute them is included in Appendix B.

Table 4.5: Cathode mass loss rate per unit power delivered.

	Cathode mass loss, g/kWh
Insert missing	1.2598
Insert present	3.073

4.2 Discussion

As the data illustrate, the graphite erosion rate with the insert present was an order of magnitude larger in absolute terms and three times larger in relative terms than the graphite erosion rate without the insert present. This is very surprising, as one would expect the opposite to be the case. A lower work function would indicate

lower operating temperatures, implying lower mass loss rates. Furthermore, visual inspection during operation indicated that much more ejecta was emitted during the first test than the second. However, there are several factors that may confound the measurements and need to be considered when evaluating them.

First, there was a three-week period between the first thruster firing and the mass measurements after it. During this time, the tank sat at partial vacuum without pumps running. Air leaked in over the course of those three weeks and brought the internal pressure up to about 30 torr. As such, when opening, the cathode had been exposed to fluctuating concentrations of water vapor for three weeks before the mass measurement was taken. As graphite absorbs water from the air, it is possible that the reason the change in mass with no emitter was so much smaller than that with was due to water absorption over those two weeks.

Second, a displacement of mass from the graphite to the insert may have contributed to the large loss of mass between the first and second measurements. After removal from the tank the second time, the insert was inspected before it was massed. There was a black coating on the first quarter of the insert near the orifice, while the rear was still a normal purple. Therefore, there is a chance that LaB_6 may have been eroded during the second operation, but an equal mass of graphite was deposited from the cathode to the insert, making its change in mass within the error of the measurement.

Third, it is possible that a current density that was too high caused the erosion. In the case of the emitter, if we assume that the current drawn was 100 A, and the emitter only emitted over a quarter of its total length, we find that the current density was approximately 250 A/cm^2. At this density, the ablation rate for LaB_6 is approximately $1x10^{-4}$ $g/cm^2/s$. [4] From these, we can find that the amount expected to be lost over the course of the second firing is approximately .0589 g. This is an order of magnitude smaller than the amount of graphite mass lost during the second firing, but could in combination with some loss of graphite onto the insert plausibly account for the lack of mass change in the insert. An equivalent current in the non-insert case would create a current density of 22.051 A/cm^2 assuming the entire orifice plate emitted electrons. This would create an evaporation rate of $1.294x10^{-4}$ g/cm^2, [13] which translates to a mass loss of .082 g. This is close to the mass lost in the first experiment, which lends credibility to the current density argument. However, as the same argument cannot explain the lack of change in the second firing, it needs to be considered in tandem with other factors. Also, if the water vapor theory is true, it means that the matching values for mass loss are just a coincidence. As such, further

study is needed to investigate mass loss in graphite OHCs.

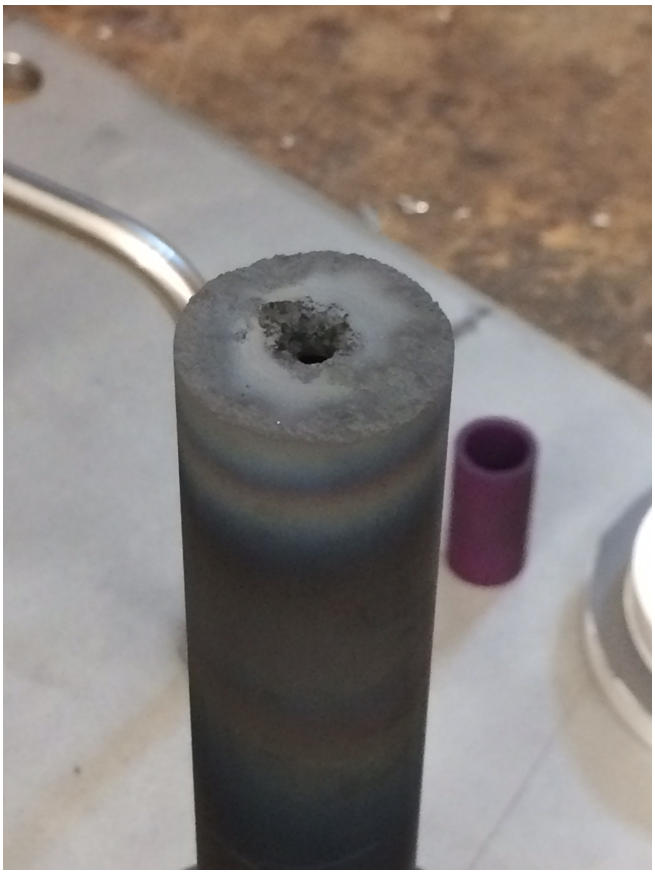

Figure 4.7: Wear on the cathode tip after 10 mins of operation without the insert in place. Note the lack of sharp edges around both the orifice and the outer edges — arcs have attached to them all and evaporated them off.

4.3 Future Work

Further work would be of much benefit in several areas. First, a redesign of the whole thruster setup to include a keeper would be beneficial. A keeper would have solved some of the initial material ejection problems when the insert was not present, and during operation, it would have guarded the cathode from bombarding ions that may have been the cause of the loss in mass. However, this would require more-or-less starting from scratch in regards to thruster design, and would take a significant amount of engineering effort, for the reasons mentioned previously.

Second, research into the reactions between graphite and boron would also be important in determining long-term cathode life. Goebel and Katz mention that

successful deployment of LaB_6 requires consideration of how to prevent boron dispersion from occurring at high temperatures [4], and little research has been done on graphite-boron relations at high temperatures. On the timescale of laboratory work, the reaction may be negligible, but on the timescale of spacecraft operation, it may change the graphite's properties, potentially shortening the lifespan of the cathode. An understanding of how the two react with each other would further hollow cathode lifetime extension research, and further the readiness of MPDTs for use in space missions.

4.4 Concluding Remarks

Ultimately, it is unclear whether or not graphite is a suitable material for MPD OHC use. The presence of the insert increased the erosion rate of the graphite by a significant margin. However, beyond that, it was shown that a working MPD cathode can be made of graphite. The presence of the emitter was (indirectly) shown to reduce the operating temperatures of the cathode, and the geometry was able to produce thrust. Further research is necessary to determine the cause of the ablation and various methods for its mitigation, as well as more general research into material interactions of graphite and emitters at high temperatures, if a graphite OHC for an MPD is to become a successful piece of flight hardware.

Bibliography

[1] *Handbook of carbon, graphite, diamond, and fullerenes: properties, processing, and applications*. William Andrew, 1993.

[2] Rolled Alloys. RA 253 MA data sheet. `https://content.rolledalloys.com/technical-resources/datasheets/RA-253-MA_DS_US_EN.pdf`, April 2015.

[3] DuPont. Teflon PTFE properties handbook. `http://www.rjchase.com/ptfe_handbook.pdf`, July 1996.

[4] Dan M. Goebel and Ira Katz. *Fundamentals of Electric Propulsion: Ion and Hall Thrusters*. John Wiley and Sons, 2008.

[5] Poco Graphite. AXM-5Q graphite properties table. `http://poco.com/MaterialsandServices/Graphite/IndustrialGrades/AXF5Q.aspx`.

[6] Robert Jahn and Edgar Choueiri. Electric propulsion. *Encyclopedia of Physical Science and Technology, Third Edition*, 5:125–141, 2002.

[7] V. Kim, V. Tikhonov, and S. Semenikhin. Fourth quarterly (final) report on the stages #3C & D of the contract on the research studies, no. NASW-4851, between RIAME MAI and NASA. Technical report, Moscow Aviation Instititue, April 1997.

[8] J. M. Lafferty. Boride cathodes. *Journal of Applied Physics*, 22:299, 1951.

[9] Dan Lev. *Investigation of Efficiency in Applied-Field Magnetoplasmadynamic Thrusters*. PhD thesis, Princeton University, 2012.

[10] David R. Lide, editor. *CRC Handbook of Physics and Chemistry*. CRC Press, 77th edition, 1997.

[11] Maris Mantenieks and Roger Myers. Preliminary test results of a hollow cathode mpd thruster. *Proceedings of the 22nd International Electric Propulsion Conference*, 1991.

[12] Matthew L. Plasek. The RF-controlled cathode: Modeling and large-diameter cathode experimental results. Master's thesis, Princeton University, `http://alfven.princeton.edu/publications/thesis/plasek-thesis-2016`, January 2016.

[13] L. B. Tecchio, M. Tonezzer, J. Bermudez, M. Loriggiola, and M. Lollo. Measurement of graphite erosion rate. *LNL Annual Report*, 2008.

[14] S. F. Vogel. Pyrolytic graphite in the design of a compact inert heater of a lanthanum hexaboride cathode. *Review of Scientific Instruments*, 41(4):585–7, 1970.

[15] Szymon Wojciechowski, Pawel Twardowski, and Marcin Pelic. Cutting forces and vibrations during ball end milling of inclined surfaces. *6th CIRP International Conference on High Performance Cutting*, 2014.

Appendix A

Manufacturing Drawings

Included in this appendix are manufacturing drawings for the cathode, anode, separator, cathode plate, anode plate, and lock ring.

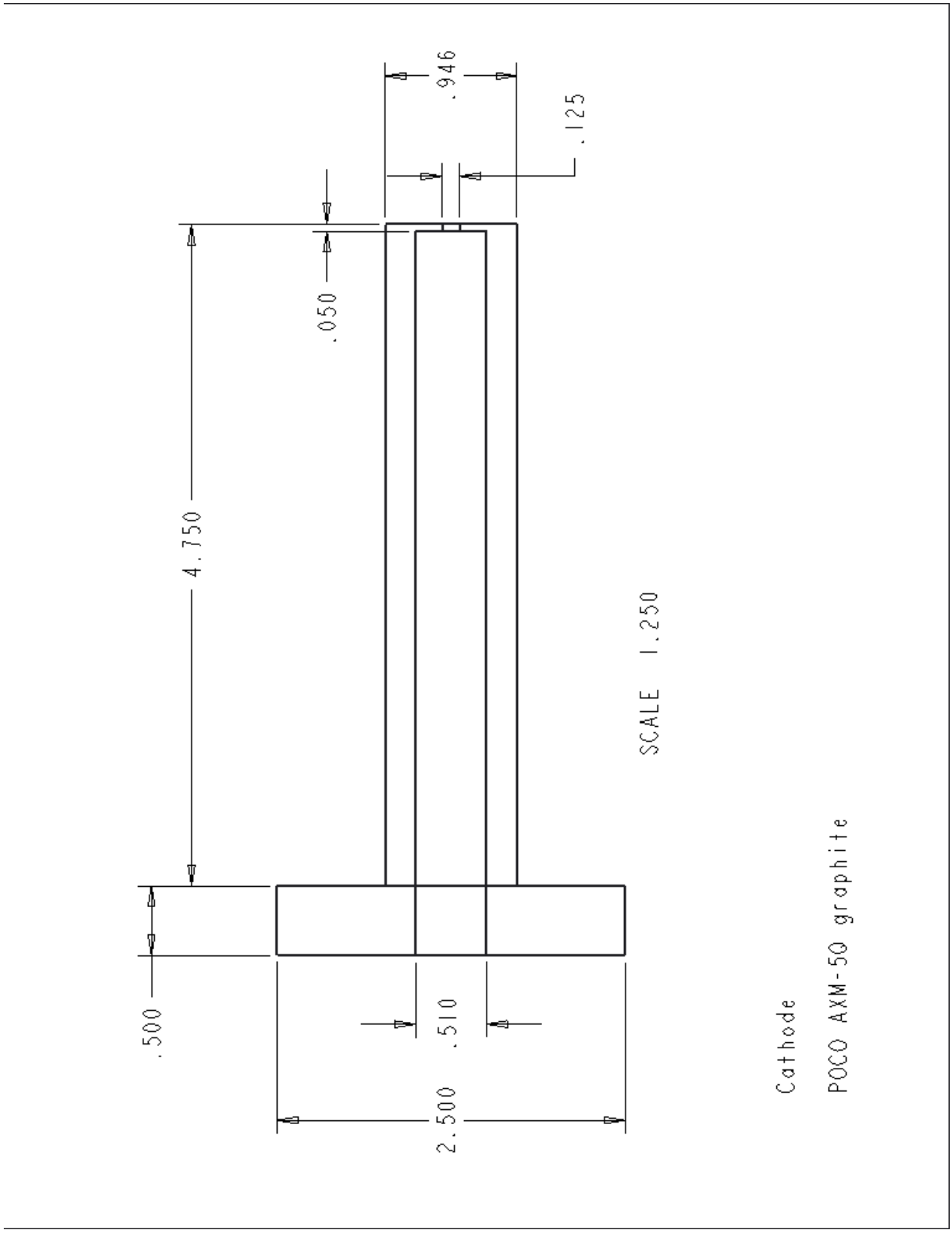
.946
.125
.050
4.750
.500
.510
2.500
SCALE 1.250
Cathode
POCO AXM-50 graphite

Anode SCALE 0.700

POCO AXM-5Q graphite

The inner curve follows the following equations, where x lies along the centerline, x = 0" at the base of the flange and x = 7.375" at the tip:

0 < x < 2.189: y = 1.5

2.189 < x < 3.688:
y = .6255*cos((pi/1.5)*x)+1.19725

3.688 < x < 4.189: x = 1.1575

4.189 < x < 7.375:
y = .063^3/(.063^2 + (.0254*(x-4.189))^2)^1.5

The outer curve is created by adding .283" to the value computed in the above equation.

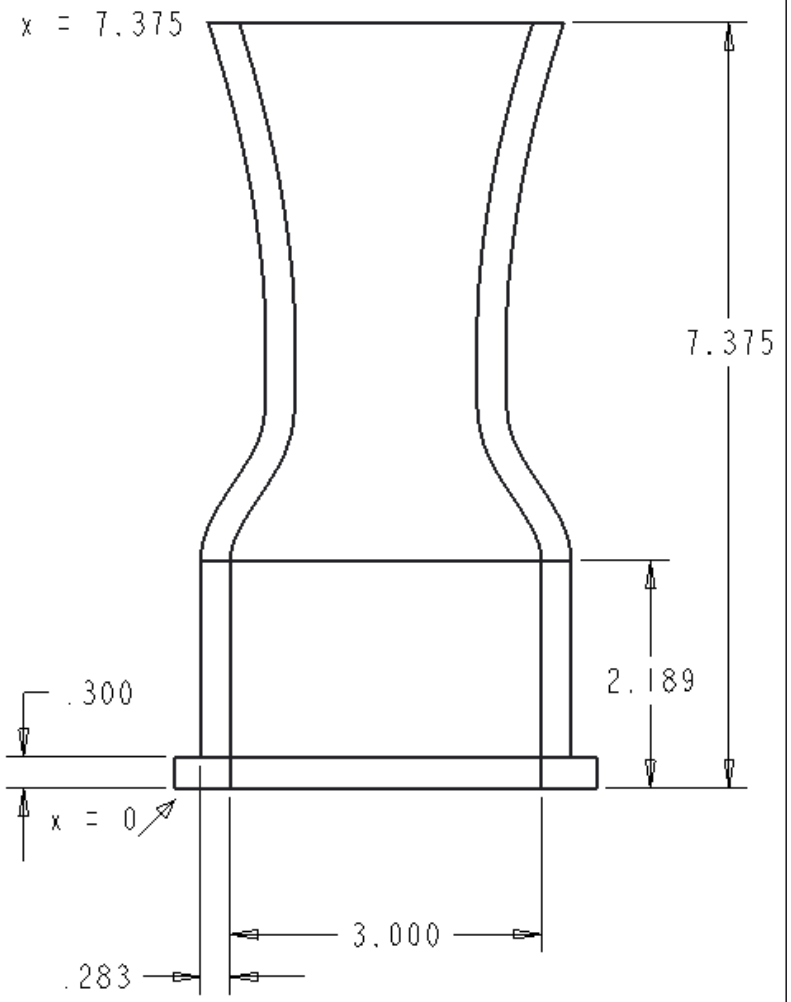

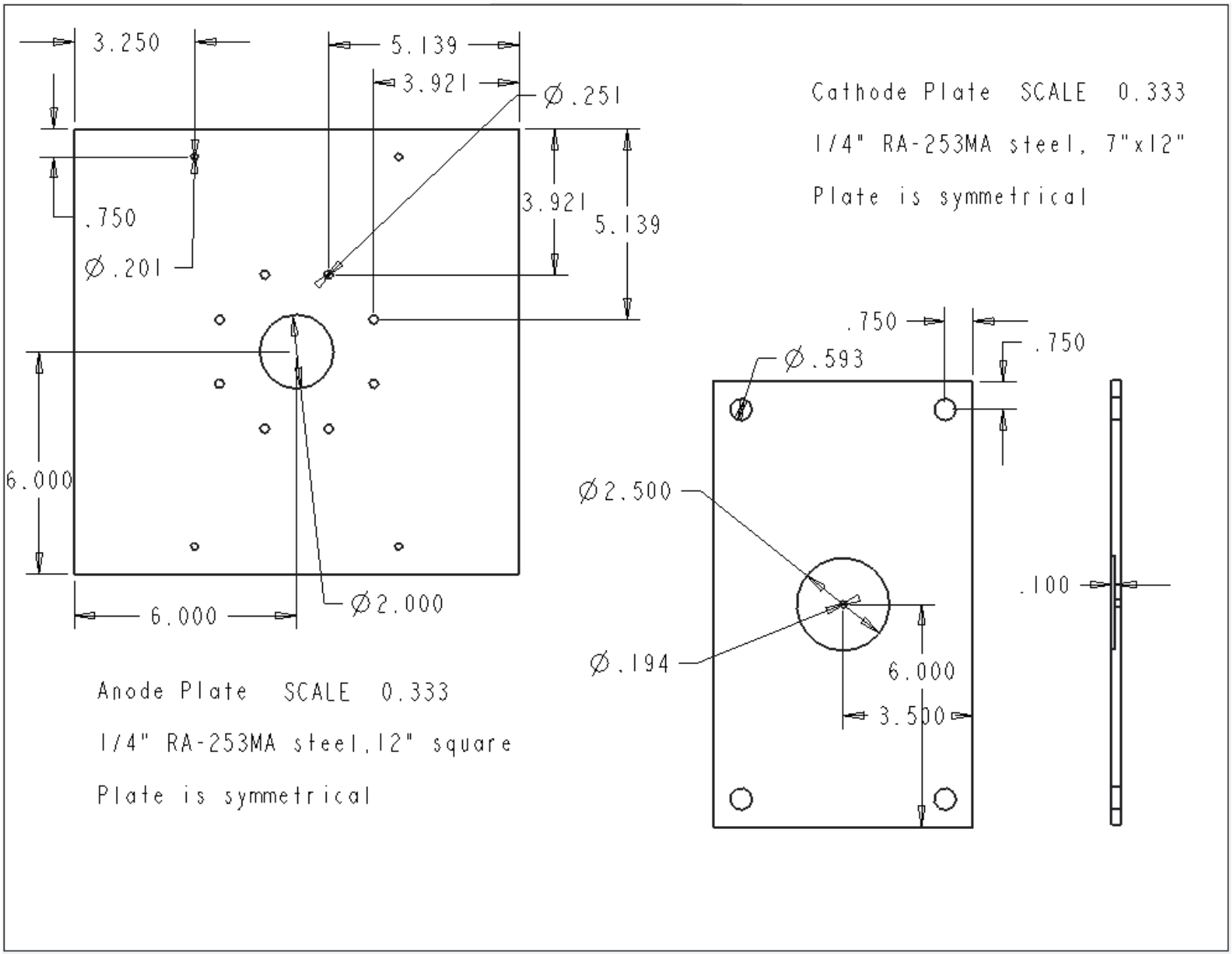
3.250
5.139
3.921
Ø.251
.750
Ø.201
3.921
5.139
6.000
Ø2.000
6.000
Anode Plate SCALE 0.333
1/4" RA-253MA steel, 12" square
Plate is symmetrical
Cathode Plate SCALE 0.333
1/4" RA-253MA steel, 7"x12"
Plate is symmetrical
.750
.750
Ø.593
Ø2.500
Ø.194
6.000
3.500
.100

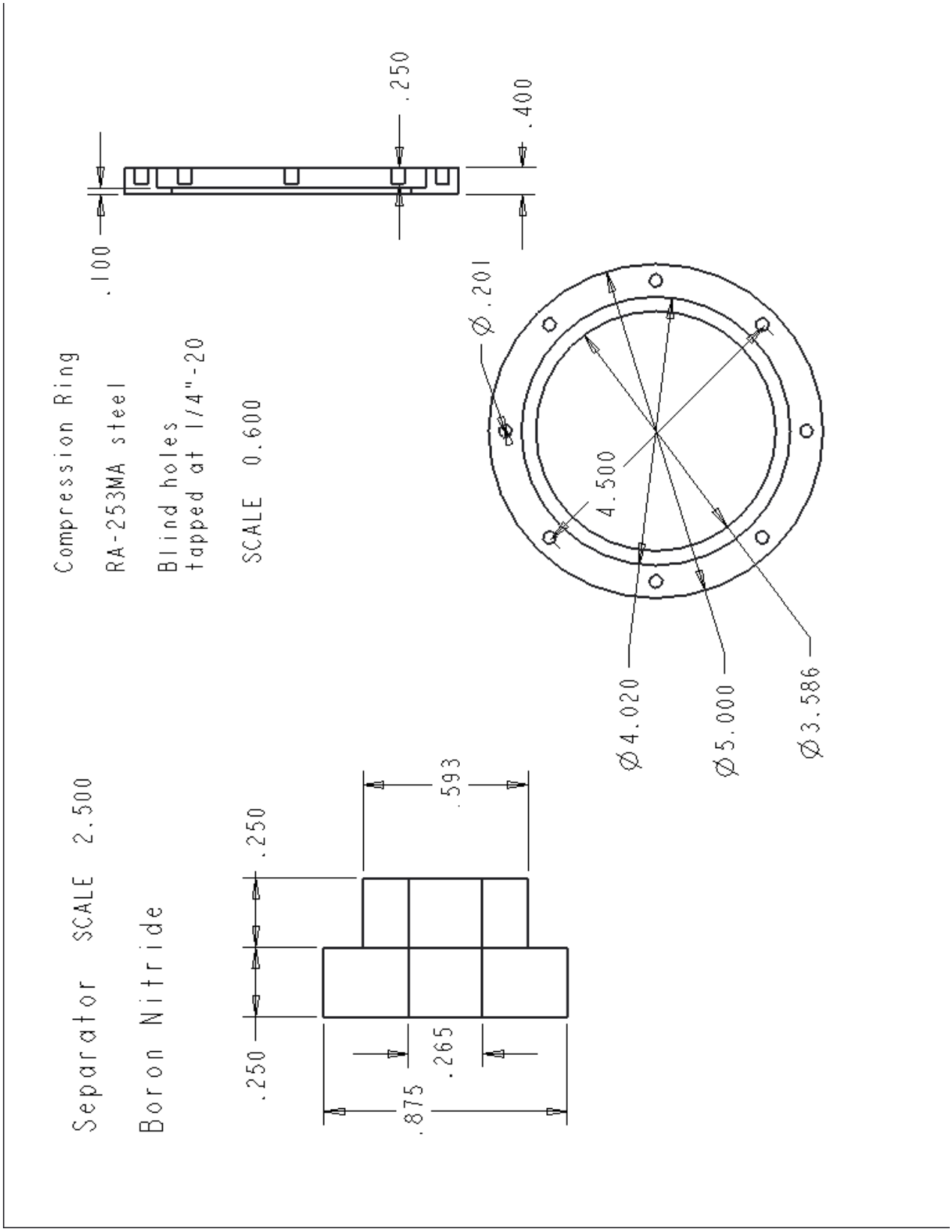
Compression Ring
RA-253MA steel
Blind holes
tapped at 1/4"-20
SCALE 0.600
.100
.250
.400
Ø.201
4.500
Ø4.020
Ø5.000
Ø3.586
Separator SCALE 2.500
Boron Nitride
.250
.250
.593
.265
.875

Appendix B

Matlab Code for Data Processing

```
% read in data from calculations_wo_insert.xlsx
% alternately read in from calculations_w_insert.xlsx
% name the four columns 'time', 'current', 'voltage', and
   'power'

op_power = power(current > 40); % over 40 A cuts out low-I
    noise from the sensor
op_time = time(current > 40);

energy = 0;
delta = [];

for i = 1:(numel(op_power)-1)
    if abs(op_time(i+1) - op_time(i)) > 2
        delta_t = .5;
    else
        delta_t = op_time(i+1) - op_time(i);
    end
```

```
    delta = [delta; delta_t];

    energy = energy + op_power(i)*delta_t;

end

% Energy is in W-s

energy = energy/(1000*3600); % 1000 W/kW, 3600 s/hr

m_lost = .098; % as measured, for no insert - use .572
   with insert

m_per_kWh = m_lost/energy;
```